HIPPARCOS ON-BOARD ATTITUDE DETERMINATION

W W Black

Formerly With:
British Aerospace Plc
Space and Communications Division
Filton
Bristol

W Salter

British Aerospace Plc
Space and Communications Division
Filton
Bristol

ABSTRACT

A necessary requirement for a satellite (such as HIPPARCOS) performing an astrometric mission, to be able to produce very high accuracy data on star position and proper motions, is high precision on-board attitude determination. This paper outlines the derivation of the HIPPARCOS on-board attitude determination algorithm which is required to give an estimate of the payload pointing to within 1 arcsec RMS. It then describes how the predicted performance of the sub-optimum Kalman Filter based algorithm was assessed by computer simulation. Finally, it discusses the performance of the algorithm predicted by the simulation, with particular emphasis placed on those factors which have a major impact on the characteristics of the performance.

KEYWORDS: HIPPARCOS, ATTITUDE DETERMINATION, KALMAN FILTER.

1. THE MISSION

Hipparcos (HIgh Precision PARallax COllecting Satellite) is the first satellite dedicated to an astrometric mission. The main mission goal is, over a period of 2½ years, to completely scan the celestial sphere 5 times and thereby produce a global star catalogue of 100,000 pre-selected stars. The position and parallax accuracy will be of the order of 2 milliarcsec, and the proper motions will be determined to 2 milliarcsec/sec. (By way of illustration of the Hipparcos accuracy, 1 milliarcsec is the approximate angle subtended to an observer on the Earth of a man on the moon).

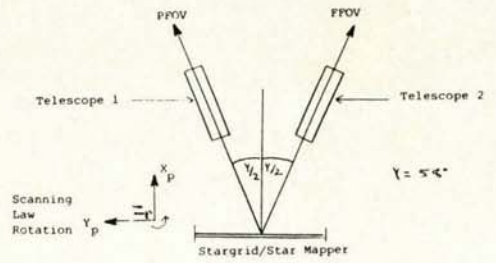

Figure 1: Definition of telescope FOV's

The Hipparcos satellite will be launched in 1988 by Ariane, and will operate in geostationary orbit. The scientific payload consists of a Schmidt-type 290mm aperture, all-reflecting telescope. Light from two Fields Of View (FOV) is conveyed through two baffles 58° apart and projected via a beam combiner onto a star grid, see Figure 1. The star grid FOV is 0.9° x 0.9°, and the Image Dissector Tube (IDT) beam which is piloted over the grid to observe the stars of interest has a 37 arcsec instantaneous FOV.

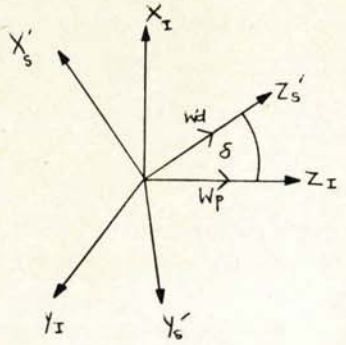

Figure 2: Definition of Nominal Scanning Law

Scanning of the celestial sphere is achieved by a coning motion as defined in Figure 2, namely:

(i) the spin axis direction (perpendicular to the two FOV's) subtends an angle, δ, of 43° with respect to the sun direction and precesses round this 43° cone with a rate Ω_d of 6.51± 1.25°/day,

(ii) additionally the spacecraft spin rate with respect to inertial space, ω_z, is maintained at 168.75°/hour.

A simplified diagram of the spacecraft configuration is given in Figure 3. The spacecraft reference frame [Xs, Ys, Zs] and the payload reference frame [X_p, Y_p, Z_p] are also defined in the Figure 3.

Proceedings of the Second International Symposium on Spacecraft Flight Dynamics, Darmstadt, FR Germany, 20–23 October 1986 (ESA SP-255, Dec. 1986)

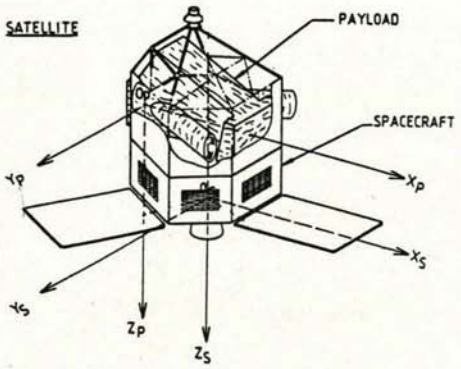

Figure 3: Definition of spacecraft and payload reference frames.

2. AOCS REQUIREMENTS FOR SCIENTIFIC MISSION PHASE

As a result of the above mission objectives the following AOCS requirements are generated.

2.1 Attitude Control.

The AOCS shall control the satellite to follow the Nominal Scanning Law (NSL) or desired motion defined above such that:

(i) the maximum error cone semi-angle of the spin axis is less than 10 arcmin

(ii) the maximum angular error about the spin axis is less than ± 10 arcmin

(iii) this control is achieved with minimal payload jitter impact.

2.2 Attitude Determination.

The AOCS shall estimate the telescope Proceeding Field of View (PFOV) and Following Field of View (FFOV) direction relative to the ideal directions to within 1 arcsec RMS.

The PFOV and FFOV angular rates relative to the ideal rates will be derived with an accuracy better than 0.14 arcsec/sec.

3. AOCS DESIGN FOR SCIENTIFIC MISSION PHASE

3.1 Attitude Control

Three axis control of the spacecraft is achieved by means of a cold gas RCS providing typically 0.020 N thrust. This solution leads to specific constraints on actuation duration (0.5 seconds maximum) and interval (not less than 100 seconds between successive actuations) as a result of payload jitter considerations.

The spacecraft 3-axis control is supervised by the Normal Mode Control (NMC) algorithm operating within the Control Law Electronics (CLE), a Texas 9989 microprocessor with 32 bit floating point arithmetic in software. Information of spacecraft attitude and rates provided by the on-board attitude determination algorithm are computed as an error function for each axis and compared with a threshold. In the event of one axis threshold crossing, then control action is initiated about all 3 axes and performed simultaneously to maximise the interval between actuations. The control philosophy is to drive the attitude error to zero after some predefined time, tp. This parameter is selected to ensure that the 100 second minimum actuation interval requirement is met. The thruster on time for each axis is calculated based on the attitude and rate estimates at the time of actuation, an on-board estimate of the mean disturbance torques over the interval tp (due to solar radiation pressure and gyro torques), and also accounts for the angular acceleration available from each thruster.

Assessment of the NMC algorithm performance during the Engineering Model (EM) study predicts typical mean actuation intervals of the order of 500-700 seconds, with expected minimum intervals not less than 175 seconds.

3.2 Attitude Determination

On-board attitude estimates of the spacecraft attitude and rate with respect to the NSL are provided by the Real Time Attitude Determination (RTAD) algorithm. This algorithm is located with the NMC algorithm in the CLE CPE microprocessor. The attitude information is used by the NMC algorithm to enable the payload IDT beam to be piloted over the star grid.

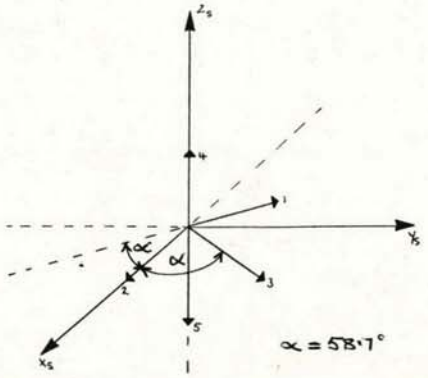

Figure 4: Gyroscope sensitive axes

The RTAD algorithm utilises inertial attitude information provided by the Inertial Reference Unit (IRU), which consists of 3 operational (and 2 redundant) single degree of freedom rate integrating torque rebalanced gyros and the associated electronics. Figure 4 indicates the sensitive axes of the 5 gyros. 2 gyros are selected from the transverse (XY plane) set (1, 2, 3) and 1 from the Z-axis set (4, 5). This allows 3-axis attitude and rate information to be derived from the Gyro Cyclic Data Acquisition Software within the CLE.

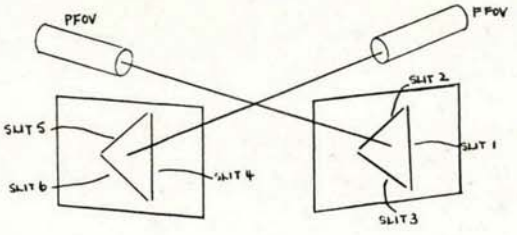

Figure 5: Definition of SM virtual slit.

The above process is supplemented by optical information provided by a Star Mapper (SM). 2 SMs (1 operational and 1 redundant) are located at either side of the star grid within the payload. Each SM consists of 3 sets of slits, (see Figure 5), two at an angle of 45° to the transverse plane and the third parallel to the Z-axis (and therefore perpendicular to the transverse plane). Stars in either FOV may be detected by both Star Mappers. Processing of the Star Mapper data within the On-Board Computer (OBC) allows a measure of the spacecraft attitude error to be calculated. This processing consists essentially of calculating the angular error equivalent to the difference between the actual star detection time and the predicted star detection time, assuming the spacecraft is following the NSL perfectly. This predicted star detection time, and other detection information is calculated on ground and uplinked to the satellite in the Program Star File (PSF) data block.

The RTAD algorithm is of Kalman filter form, where the inertial information represents the process and the optical information represents the measurement. The filter is of sub-optimum form, where the gains associated with the SM measurement are not computed recursively, based on the error covariance matrix, but constant values are utilised. These constant values are the average gains derived from equivalent optimum filter computer simulations.

3.2.1 Derivation of the RTAD Filter Formation. A summary of the RTAD filter derivation from the spacecraft motion relative to the NSL trajectory is provided below to facilitate discussion of the performance later in the paper.

The RTAD algorithm estimates the attitude and rates of the spacecraft reference frame [X_s, Y_s, Z_s] defined in Figure 3 with respect to the NSL reference frame, i.e. the spacecraft reference frame position with respect to inertial space were the spacecraft following the NSL trajectory perfectly, [X'_s, Y'_s, Z'_s]. The relative attitude (or attitude error) may be expressed by an angle rotation set, the one chosen for this application being the Tait-Bryan angles [ϕ, θ, ψ]. This allows the NSL reference frame to be transformed into the spacecraft reference frame by 3 sequential rotations, ψ about Z'_s to produce the first intermediate axis set [X''_s, Y''_s, Z''_s] then θ about Y'' to produce [X'''_s, Y'''_s, Z'''_s] and finally ϕ about X'''_s.

The NSL reference frame rates (expressed in NSL reference frame axes) with respect to inertial space are defined by ($\omega x, \omega y, \omega z$). The spacecraft body rates w.r.t inertial space expressed in spacecraft reference frame axes are subsequently defined by [p, q, r].

3.2.1.1 The Gyro Based Estimation Process. The spacecraft kinematics are given by:

$$\dot{\phi} = p\frac{\cos\psi}{\cos\theta} - q\frac{\sin\psi}{\cos\theta} - \omega x - \tan\theta(\omega y\sin\phi - \omega z\cos\phi) \quad (1)$$

$$\dot{\theta} = p\sin\psi + q\cos\psi - (\omega y\cos\phi + \omega z\sin\phi) \quad (2)$$

$$\dot{\psi} = r + \tan\theta(q\sin\psi - p\cos\psi) + \frac{1}{\cos\theta}(\omega y\sin\phi - \omega z\cos\phi) \quad (3)$$

The rates (ωx, ωy, ωz) are derived from the NSL definition and are therefore fully deterministic. These rates are calculated within the RTAD from uplinked NSL parameters. Estimates of the absolute spacecraft rotation rate (p, q, r) are derived by pre-processing the gyro outputs within the CLE, to transform the information provided by the IRU in gyro input axes to spacecraft reference frame axes. These estimates are corrupted by measurement noise associated with the gyros. For the purposes of this derivation two sources of noise are considered:

(i) gyro drift noise d, assumed to be a Wiener process (integrated white noise, i.e. $d = \int n$) with associated Power Spectral Density $Q_n = 10^{-19}$ rad^2/sec^3/Hz (4)

(ii) gyro rate noise r, within "average" PSD $Q_r = 10^{-3}$ (°/hour)^2/Hz (5)

Then the pre-processed gyro outputs may be related to the spacecraft body rates by the following equations:

$$\tilde{p} = p + dx + rx \quad (6)$$

$$\tilde{q} = q + dy + ry \quad (7)$$

$$\tilde{r} = r + dz + rz \quad (8)$$

where ($\tilde{p}$, $\tilde{q}$, $\tilde{r}$) are the pre-processed gyro outputs

(dx, dy, dz) are the virtual gyro drifts (i.e. gyro drifts expressed in spacecraft axes)

(rx, ry, rz) are the virtual gyro rate noise (i.e. expressed in spacecraft axes)

Incorporation of equations (6) - (8) in (1) - (3) defines the continuous gyro estimation process. The continuous filter formulation is derived by noting the following,

(i) the performance is improved if the gyro drift is included in the state vector, i.e. the state vector becomes [ϕ, θ, ψ, dx, dy, dz]

(ii) by the AOCS requirement ϕ, θ, ψ must be less than 10 arcmin. Consequently it is possible to take truncated power series expansions for the trigonometric functions.

(iii) ignore terms which contribute 0.1 arcsec or less over 100 seconds.

These considerations lead to the following definition of the gyro based estimation process:

$$\begin{bmatrix}\phi\\ \theta\\ \psi\\ dx\\ dy\\ dz\end{bmatrix} = \begin{bmatrix} 0 & \omega z & 0 & -1 & 0 & 0\\ -\omega z & 0 & 0 & 0 & -1 & 0\\ 0 & 0 & 0 & 0 & 0 & -1\\ 0 & 0 & 0 & 1 & 0 & 0\\ 0 & 0 & 0 & 0 & 1 & 0\\ 0 & 0 & 0 & 0 & 0 & 1\end{bmatrix}\begin{bmatrix}\phi\\ \theta\\ \psi\\ dx\\ dy\\ dz\end{bmatrix} + \begin{bmatrix}(\tilde{p}-\omega x)-(\tilde{q}-dx)\phi\\ (\tilde{q}-\omega y)+(\tilde{p}-dx)\phi\\ (\tilde{r}-\omega z)-(\tilde{p}-dx)\theta\\ 0\\ 0\\ 0\end{bmatrix} + \begin{bmatrix}-rx+ry.\psi\\ -ry-rx.\psi\\ -rz+rx.\theta\\ nx\\ ny\\ nz\end{bmatrix} \tag{9}$$

or $$\underline{\dot{X}}(t) = A\underline{X}(t) + B\underline{U}(t) + \underline{W}(t) \tag{10}$$

where $\underline{X}(t)$ = state vector

A = state matrix

B = control matrix

$\underline{U}(t)$ = control vector

$\underline{W}(t)$ = system noise process vector

To implement the above formulation on a digital computer it is necessary to derive the equivalent discrete system representation:

$$\underline{X}(t_{k+1}) = F(t_{k+1}, t_k)\underline{X}(k) + G(k)\underline{U}(t_k) + \underline{\nu}(k+1) \tag{11}$$

where $\underline{X}(t_{k+1})$ = state vector at time t_{k+1}

$\underline{X}(t_k)$ = state vector at previous time t_k

$F(t_{k+1}, t_k)$ = state transition matrix

$$G(k) = \int_{t_k}^{t_{k+1}} F(t_{k+1}, \tau).B(\tau).d\tau$$

$$\underline{\nu}(k+1) = \int_{t_k}^{t_{k+1}} F(t_{k+1}, \tau).W(\tau).d\tau$$

By the above method, and again noting (ii) and (iii) from the continuous derivation, the equivalent discrete formulation of equation (9) is given by:

$$\begin{bmatrix}\phi(k+1)\\ \theta(k+1)\\ \psi(k+1)\\ dx(k+1)\\ dy(k+1)\\ dz(k+1)\end{bmatrix} = \begin{bmatrix} 0 & \omega zT & 0 & -T & 0 & 0\\ -\omega zT & 0 & 0 & 0 & -T & 0\\ 0 & 0 & 0 & 0 & 0 & -T\\ 0 & 0 & 0 & 1 & 0 & 0\\ 0 & 0 & 0 & 0 & 1 & 0\\ 0 & 0 & 0 & 0 & 0 & 1\end{bmatrix}\begin{bmatrix}\phi(k)\\ \theta(k)\\ \psi(k)\\ dx(k)\\ dy(k)\\ dz(k)\end{bmatrix} + \begin{bmatrix}Gx(k+1)-\omega x(k)T-\psi(k)Gy(k+1)\\ Gy(k+1)-\omega y(k)T+\psi(k)Gx(k+1)\\ Gz(k+1)-\omega z(k)T-\theta(k)Gx(k+1)\\ 0\\ 0\\ 0\end{bmatrix} + \underline{\nu}(k+1) \tag{12}$$

$$\underline{X}(k+1) = F(t_{k+1}, t_k).\underline{X}(k) + \underline{\Gamma}(k+1) + \underline{\nu}(k+1) \tag{13}$$

where $$Gx(k+1) = \int_{t_k}^{t_{k+1}} \tilde{p}(\tau).d\tau \text{ etc} \tag{14}$$

$$\tau = t_{k+1} - t_k \text{ (recursion time step)} \tag{15}$$

To arrive at the filter formulation note that (rx, ry, rz) and (wx, wy, wz) of $\underline{W}(t)$ are zero mean white noise processes of Gaussian distribution. Further due to the magnitude of the control law angles (<600 arcsec) we can assume

$$ry.\psi << rx \text{ etc}$$

Then the expected value of $\underline{\nu}(k+1)$, i.e. $E[\underline{\nu}(k+1)]$ is zero. Therefore the RTAD gyro based estimation process is given by

$$\hat{\underline{X}}^{-}(k+1) = F(t_{k+1}, t_k).\hat{\underline{X}}^{+}(k) + \underline{\Gamma}(k+1) \tag{16}$$

where the superscript ^ denotes estimated quantities.

3.2.1.2 The Star Mapper Measurement Equation.

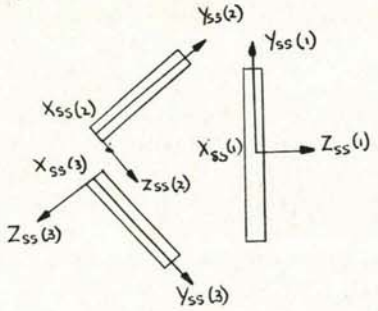

Figure 6: Definition of SM slit reference frames.

The Star Mapper receives information from both FOVs and can therefore be considered as 6 virtual slits as defined in Figure 5. By defining Slit Reference Frames for each virtual slit (as indicated in Figure 6), then the mathematical criteria for a star to be observed by slit i is

$$\underline{S}.\underline{Z}_{ss}(i) = 0 \tag{17}$$

$$\beta_1 \leq \underline{S}.\underline{Y}_{ss}(i) \leq \beta_2 \tag{18}$$

where $\underline{S}$ = star vector

$\underline{Z}ss$ = slit z-axis vector

β_1, β_2 = limits of the slit FOV

The predicted star crossing time has the same criteria, in particular

$$\underline{S}.\underline{Z}'_{ss}(i) = 0 \tag{19}$$

where $\underline{Z}'ss\ (i)$ = slit z-axis vector for spacecraft on NSL.

That implies that the star vector $\underline{S}$ may be expressed in "NSL" slit axes as

$$\underline{S}\,|_{ss} = (\cos\delta, \sin\delta, 0)^T \tag{20}$$

where δ = elevation of star in slit FOV.

The measurement equation is derived by defining in the actual slit reference axes by the following transformation

$$\underline{S}|_{ss} = [\Delta][T][NSL(td-tp)][\Delta]^T \underline{S}_{ss} \quad (21)$$

where $[\Delta]$ = 3x3 orthogonal transformation matrix from spacecraft to slit axes

$[T]$ = $[\Phi]$ $[\theta]$ $[\psi]$ = transformation matrix from nominal to actual spacecraft axes

$NSL(td-tp)$ = transformation matrix from NSL axes at time tp to time td

Then if $\underline{S}|_{ss} = (Sx, Sy, Sz)^T$ the detection criterion of equation (17) implies

$$Sz = 0 \quad (22)$$

Equation (21) may be reduced by small angle approximations to the form

$$\omega z.\tau + \Delta Y = -\tan\Delta_2.(\sin\Delta_1.\Phi - \cos\Delta_1.\theta) - \psi \quad (23)$$

$$\equiv (-\tan\Delta_2.\sin\Delta_1, \tan\Delta_2\cos\Delta_1, -1, 0, 0, 0)^T.\underline{X} \quad (24)$$

where ωz = spin rate

ΔY = correction term applied for non-linear and second order terms

(Δ_1, Δ_2) = transformation angles between spacecraft axes and slit axes

or $$Y \equiv \omega z.\tau + \Delta Y = Mi.\underline{X} \quad (25)$$

where Mi = Measurement Matrix for slit .

By applying the correction term ΔY the scalar quantity calculated by the OBC is a linear function of the state vector $\underline{X}$ as shown in equation (24).

The OBC passes across the scalar quantity ΔY to be used by the RTAD algorithm. Due to the variable update due to SM/OBC processing and algorithm activation frequency (0.5 to 2.0 seconds), the scalar quantity is extrapolated to the RTAD algorithm estimate update time. The RTAD measurement estimate (based on the attitude error estimates ϕ, θ, ψ) is subtracted from this extrapolated value and the state vector updated using this quantity. The selection of the gain is discussed later.

The update equations are then given by

$$Yi(tu) = Yi(td) + \frac{tu-td}{\Delta T} Mi.[\hat{\underline{X}}^-(k+1) - \hat{\underline{X}}^+(k)] \quad (26)$$

where Yi(tu) = measurement extrapolated to time tu

ΔT = RTAD activation time step

$$\hat{\underline{X}}^+(k+1) = \hat{\underline{X}}^-(k+1) + Ki.[Yi(tu) - Mi.\hat{\underline{X}}^-(k+1)] \quad (27)$$

where $\hat{\underline{X}}^+(k+1)$ = State Vector Estimate after update

$\hat{\underline{X}}^-(k+1)$ = State Vector Estimate prior to update

Ki = 6 x 1 gain matrix associated with slit i.

A point of interest concerns the information provided by the vertical or slanted slits. Due to the transformation from spacecraft axes to virtual slit axes the generalised measurement equation for the slanted virtual slits (2, 3, 5, 6) is given by [from equations (24) and (25)]

$$\underline{Y} \equiv (\sin 29°, \cos 29°, -1, 0, 0, 0)^T.\underline{X} \quad (28)$$

where the sign (±) is determined by the slit.

In physical terms the measurements from the slanted slits (2, 3, 5, 6) provide information about all 3 axes.

However, the measurement equation for the vertical virtual slits (1, 4) is given by

$$\underline{Y} \equiv (0, 0, -1, 0, 0, 0)^T.\underline{X} \quad (29)$$

and therefore vertical slit measurements only provides information about the z-axis.

Summarising the RTAD algorithm

Gyro Based Estimation Process

$$\hat{\underline{X}}^-(k+1) = F(t_{k+1}, t_k).\hat{\underline{X}}^+(k) + \underline{\Gamma}(k+1) \quad (30)$$

No SM Measurement Available

$$\hat{\underline{X}}^+(k+1) = \hat{\underline{X}}^-(k+1) \quad (31)$$

SM Measurement Available

$$Yi(tu) = Yi(td) + \frac{tu-td}{\Delta T} Mi.[\hat{\underline{X}}^-(k+1) - \hat{\underline{X}}^+(k)] \quad (32)$$

$$\hat{\underline{X}}^+(k+1) = \hat{\underline{X}}^-(k+1) + Ki.[Yi(tu) - Mi.\hat{\underline{X}}^-(k+1)] \quad (33)$$

The Rate Estimation Process is based on successive attitude estimates, i.e.

$$\hat{\underline{X}}^+(k+1) = \frac{\hat{\underline{X}}^-(k+1) - \hat{\underline{X}}^+(k)}{\Delta T} \quad (34)$$

3.3 RTAD/NMC Computer Simulation

The only representative method by which the RTAD performance may be assessed is by closed loop computer simulation of the NMC and RTAD. The simulation philosophy is as given below:

(1) Based on star statistics provided by ESTEC, a star skyslice (an annulus of the celestial sphere, 360° by 2°) is generated. This is used to generate the predicted star detection times used for the PSF by determining the idealised FOV trajectory over the skyslice.

(2) The above model skyslice is then "corrupted" to produce a "real" skyslice according to each star's a-priori position error for use within the simulation. Each star position is randomly shifted according to the Guassianly distributed standard deviation.

(3) SM/OBC processing errors, which are a function of the star characteristics and the slit which obtains the information, are generated randomly according to the error standard deviation distribution. This allows an actual detection time to be computed within the simulation. The RTAD/NMC simulation block diagram is presented in Figure 7. The orbital oscillator algorithm generates the trigonometric functions required within the RTAD algorithm to calculate the NSL rates and within the NMC algorithm to calculate the solar radiation pressure disturbance torque estimates.

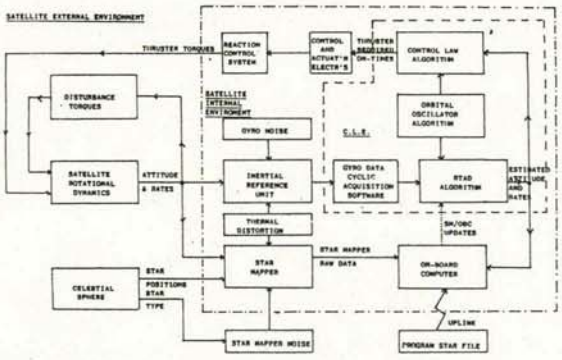

Figure 7: RTAD normal mode simulation block diagram.

The structural distortion between the payload reference frame and IRU reference frame due to thermal effects is included in the block "Thermal Distortion". This model will be discussed later in this paper since this error source drives the RTAD performance.

4. RTAD PERFORMANCE

4.1 Phase B2 Predicted Performance And Gain Selection

The performance of the RTAD during Phase B2 of the project was predicted by simulation. The mean RMS pointing estimation error for each FOV, and the associated rate estimation error were determined over 1 scan period (approximately 7680 seconds). In order to eliminate anomalies due to individual star patterns the performance measure used was the mean RMS performance (based on 10 skyslices). The performance of the optimum filter was compared with that given by a filter employing constant update gains derived from optimum filter gains averaged over several skyslices.

The B2 AOCS subsystem baseline relevant to the RTAD performance was as follows:

(1) the CLE microprocessor was a Harris 6100, a 12 bit processor. Early analysis indicated that double word length was necessary to achieve the required performance.

(2) the thermal distortion model assumed was

$$\begin{bmatrix} p \\ q \\ r \end{bmatrix} = \begin{bmatrix} 1 & \rho 1 & -\rho 2 \\ -\rho 1 & 1 & \rho 3 \\ \rho 2 & -\rho 3 & 1 \end{bmatrix} \begin{bmatrix} p' \\ q' \\ r' \end{bmatrix} \qquad (35)$$

where $[p,\ q,\ r]^T$ = body rates expressed in payload axes

where $[p',\ q',\ r']^T$ = body rates expressed in spacecraft axes

$\rho_i = \rho_o \sin(3\omega dt + \Omega i)$

$\omega d = 168.75°/hr$

Ωi = phase angle,

ρ_o = 4 arcsec/sec

(3) the SM/OBC processing RMS error, dependent on star characteristics and detecting slit, varied from 0.16 arcsec to 0.29 arcsec.

(4) the star RMS position error, again dependent on star characteristics, varied from 0.14 arcsec to 1.0 arcsec.

Using an optimum Kalman filter the mean RMS performance was determined to be

Mean RMS Pointing Estimation Error
= 0.51 arcsec

Mean RMS Pointing Rate Estimation Error
= 0.072 arcsec/sec

Utilisation of constant gains derived from the optimum simulation (averaged over several different skyslices) resulted in a degradation of the above attitude performance of the order of 25%. Given the large margin available at B2 w.r.t the AOCS specification (1 arcsec) the B2 baseline was to utilise constant gains. (NB: Optimum gains could not have been implemented within the Harris 6100 anyway due to processing constraints for an RTAD activation frequency of approximately 1Hz).

4.2 Engineering Model (EM) Predicted Performance And Gain Selection

During the Hipparcos mission the RTAD is required to perform not only in nominal sunlit operation, but also during periods of eclipse, occultation (periods during which star mapper updates are not available to the RTAD), station keeping manoeuvres and during initialisation. The time spent in these non-nominal modes is

small compared with normal sunlit operation, the percentage of the mission spent in all these modes is shown below in Table 1. The performance of the RTAD during these operations was assessed during the EM study and is discussed in the following sections.

Mode of Operation	Percentage of Mission
Occultation	5.3
Station keeping	0.003
Eclipse	1.1

Table 1

4.2.1 Sunlit Operation. The sunlit performance of the RTAD during the EM phase of the study was again predicted by simulation. The AOCS subsystem baselined for EM has several changes affecting the performance of the RTAD. The changes having most impact are discussed below:

(1) the CLE microprocessor was changed to a Texas 9989 utilising 16-bit floating point arithmetic. No appreciable effect on performance was noted.

(2) the star RMS a-priori errors were found to be worse and so increased to between 0.2 to 1.5 arcsec depending on star characteristics. This produced an 11% degradation in pointing estimate performance but no significant change in the mean RMS pointing rate estimate.

(3) the B2 gyro model was upgraded to more accurately represent gyro delays and gyro noise sources. This produced no degradation of mean RMS pointing estimate performance but did produce an approximate 60% increase in mean RMS pointing rate estimate errors.

(4) the simulation was updated to allow gyro misalignments, constant drift bias and constant scale factor errors to be modelled. A small degradation of 2% in the mean RMS pointing estimate performance was predicted for these effects.

(5) a more detailed thermal distortion model was supplied to BAe to be incorporated into the EM computer simulation. This new model considered not only external thermal distortion, whereby the gyro package distorts within the payload reference frame (as was the case in B2), but also internal distortion of the gyroscopes themselves in relation to their nominal positions in the package. The internal thermal distortion was modelled as sinusoidal of amplitude A_i and period one great circle. The external thermal distortion was modelled as sinusoidal for the X and Z axes as with B2 but with period of one great circle and amplitude B_i. It was found that the y-axis external thermal distortion could not be adequately modelled as a simple sinusoid and therefore was modelled explicitly and read into the simulation from an external data file as a series of data points.

The thermal distortion model assumed was

$$\begin{bmatrix} p \\ q \\ r \end{bmatrix} = \begin{bmatrix} 1 & \rho 1' & -\rho 2' \\ -\rho 1' & 1 & \rho 3' \\ \rho 2' & -\rho 3' & 1 \end{bmatrix} \begin{bmatrix} p' \\ q' \\ r' \end{bmatrix} + \begin{bmatrix} \dot{\rho}_1' \\ \dot{\rho}_2' \\ \dot{\rho}_3' \end{bmatrix} \qquad (36)$$

where

$$\left.\begin{aligned} \rho_i' &= (Ai+Bi)\sin(\omega d.t+\Omega i) \\ \dot{\rho}_i' &= (Ai+Bi).\omega d.\cos(\omega d.t+\Omega i) \end{aligned}\right\} \; i = x,z$$

$$\left.\begin{aligned} \rho_i' &= C + Ai.\sin(\omega d.t+\Omega i) \\ \dot{\rho}_i' &= D + Ai.\omega d.\cos(\omega d.t+\Omega i) \end{aligned}\right\} \; i = y$$

C = y-axis displacement due to external thermal distortion

D = time varying y-axis angular rate due to external thermal distortion

$(p - p')$ = drift about the x-axis due to thermal distortion

The phases Ω_i can be chosen arbitrarily (provided $\Omega_1 - \Omega_2 = 90°$) and so any choice may lead inadvertantly to particularly favourable or unfavourable conditions and hence give unrepresentative performance statistics. Therefore, for each skyslice a different set of phases, Ω_i, covering the range 0° to 360° was chosen to allow a full range of conditions to be modelled. This allowed more representative predictions of the mean RMS pointing and pointing rate estimates to be calculated by the simulation.

Using an optimum Kalman filter the mean RMS performance was determined to be

Mean RMS Pointing Estimate Error
= 0.86 arcsec

Mean RMS Pointing Rate Estimate Error
= 0.116 arcsec/sec

It can be seen that the EM study shows a substantial degradation in performance from that obtained during the B2 study. The reduced RTAD performance is due largely to the inclusion of the new thermal distortion model. The new thermal distortion model shows higher levels of distortion about all three-axes leading to increased gyro drift bias variation between star updates. The RTAD drift estimate remains constant between successive star updates and so the RTAD drift estimate does not follow the drift bias variation between updates. The spacecraft estimated attitude is derived from the gyro output minus the RTAD estimate of the drift bias - see equation (9). The RTAD drift estimate is used to compensate for the drift biases corrupting the gyro measure of the spacecraft rates and therefore the reduced accuracy of the EM drift estimate has lead to increased attitude estimate errors and hence reduced telescope pointing estimate performance.

The performance of the fixed gain filter derived in the same manner as for B2 produced a degradation of the above pointing performance of approximately 40% and therefore was outside specification. In order to meet the specification and avoid the heavy burden placed on the CLE by incorporating an optimal Kalman filter, it was decided to produce a two gain filter. To do this the stars in each PSF were divided into two categories depending on their a-priori error. Stars for which there was good confidence in their angular position (i.e. low a-priori error) were defined as category 1 stars and stars for which there was low confidence in their angular positions, as category 2 stars. For each set of stars a constant gain filter was then developed from averaged optimum filter gains. The performance determined for this two gain filter gave only a 10% degradation in mean RMS pointing estimate error over the Kalman filter employing optimum gains. This performance meets the specification and therefore a two gain filter was chosen for the EM study. The two gain filter performance determined was:

Mean RMS Pointing Estimate Error
= 0.95 arcsec

Mean RMS Pointing Rate Estimate Error
= 0.116 arcsec/sec

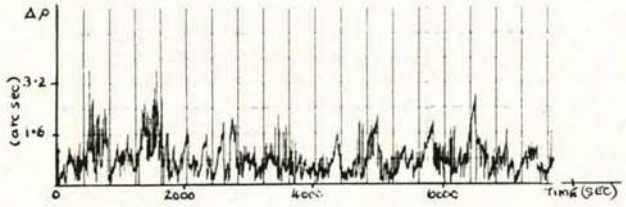

Figure 8: Pointing estimate error-sunlit operation

Δρ=Pointing estimate error

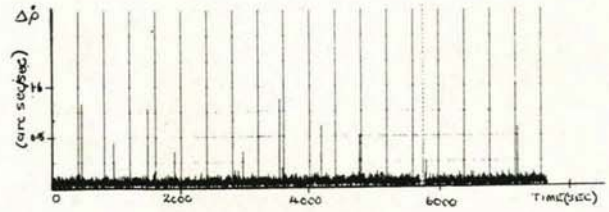

Figure 9: Pointing rate estimate error-sunlit operation

$\Delta\dot{\rho}$=Pointing rate estimate error

Figures 8 and 9 show typical pointing and pointing rate estimate errors for sunlit operations.

The above performance results were derived considering a nominal gyro configuration 124 (gyros 1, 2, and 4 operational) and the operational star mapper (OM). Two failure gyro configurations (134 and 234) and the redundant star mapper (RM) were also investigated.

The orientation of the redundant star mapper is such that the stars pass the vertical slits before reaching the inclined slits. Due to OBC SM data processing constraints any star detection occurring within 3 seconds, known as the inhibition time, of previously processed star data is ignored. Therefore the redundant SM inclined slit detection are often lost when stars have previously been detected by the vertical slit. In order to optimise the performance of the redundant SM a new set of fixed gains was calculated for category 1 and category 2 stars specifically for the redundant SM slit configuration. The vertical slit only provides ψ information, whereas the inclined slits provide ϕ, θ and ψ data. Therefore, even with optimised gains the redundant SM produced significantly reduced mean RMS pointing performance over the operational SM, by between 6% and 20% depending on the gyro configuration. Table 2 details the predicted performance for each of the failure sensor configurations.

Sensor Configuration	Mean RMS Pointing Estimate Error (arcsec)	Mean RMS Pointing Rate Estimate Error (arcsec/sec)
134OM	0.95	0.107
234OM	0.85	0.122
124RM	1.01	0.116
134RM	1.04	0.108
234RM	1.03	0.122

Table 2.

123OM: Gyro configuration 1, 2, 3 and the operational SM.

123RM: Gyro configuration 1, 2, 3 and the redundant SM.

...etc.

In order to improve the performance of the redundant SM, the star detections by the vertical slit were suppressed to allow more detections by the inclined slits and the gains were again optimised for this configuration. This was found to improve the redundant SM performance by approximately 2% for gyro configuration 124. However, a more significant improvement was found during eclipse operation, which is discussed later.

4.2.2 Eclipse Operation. An eclipse is a period during which the sun does not impinge on the satellite due to the position of the earth. Eclipses occur during short periods of the year around the equinoxes and last between 0 and 72 minutes. For the purpose of predicting the RTAD performance during eclipse a 72-minute eclipse period was assumed. The specification of RTAD performance during eclipse is the same as for normal sunlit operation.

The differences created by eclipse operation as compared with sunlit operation, were in terms of the disturbance torques and the thermal distortion. In eclipse the solar radiation pressure no longer contributes to the disturbance torque. This simply changes the motion of the satellite rather than the performance of the RTAD. However, the changes in thermal distortion as a result of eclipse entry and exit were found to drive the RTAD performance in this mode and were responsible for the reduced predicted performance shown by

Table 3.

Sensor Configuration	Mean RMS Pointing Estimate Error (arcsec)	Mean RMS Pointing Rate Estimate Error (arcsec/sec)
124OM	1.44	0.114
134OM	1.63	0.106
234OM	1.51	0.119
124RM	2.05	0.115
134RM	2.28	0.107
234RM	2.03	0.119

Table 3.

The thermal distortion model for the eclipse operation was assumed to comprise of 3 distinct phases:

(a) Up to the eclipse normal sunlit thermal distortion.

(b) For the duration of the eclipse the thermal distortion varies exponentially.

(c) Following eclipse the thermal distortion has 2 components, the normal sunlit thermal distortion and an exponential component representing the recovery from eclipse thermal distortion to normal sunlit thermal distortion.

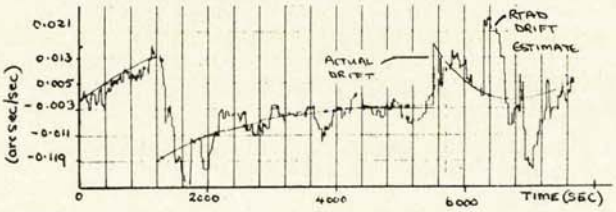

Figure 10: Z-axis gyro drift rate profile-eclipse operation

This model leads to discontinuities in gyro drift at eclipse entry and exit due to the discontinuous nature of the derivative of the thermal distortion and as a result a poor RTAD estimate was found in these regions, see Figure 10. It has already been noted that poor drift estimates lead to poor pointing performance and this was clearly shown by the poor pointing estimates in the locality of the eclipse boundaries, see Figure 11. As a result the predicted mean RMS pointing estimate errors were outside the 1 arcsec specification.

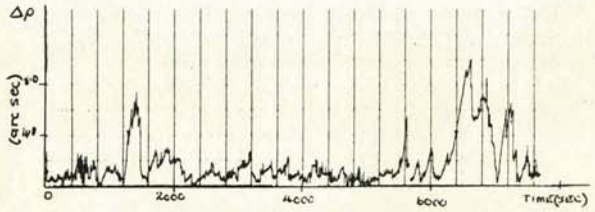

Figure 11: Pointing estimate error-eclipse operation

The limit on the instantaneous pointing estimate errors for the OBC to uniquely identify any detected star is approximately 5 arcsec in normal SM/OBC operation. The maximum predicted instantaneous pointing estimate error was 14.8 arcsec which is outside the limit of the SM/OBC normal mode. A secondary mode of SM/OBC operation exists in which a reduced number of reference stars are considered. This allows the OBC to uniquely identify stars for pointing estimate errors up to 29 arcsec. This is known as Extended Window Mode (EWM).

If the pointing estimate error were to exceed the limit of either SM/OBC operating mode, then the attitude reference would be lost. The RTAD would then require re-initialisation by ground intervention, which will be described in section 4.2.5.

The OBC star processing time and inhibition delay are increased in EWM, which in combination with the more sparse distribution of stars leads to a lower RTAD performance in this mode. However in order to accommodate the eclipse spikes it was necessary to switch to EWM.

The predicted RTAD performance for configuration 124OM in eclipse, using EWM, showed a 75% degradation on the performance given in Table 3, to 2.64 arcsec. In reality the performance in Table 3 is not achievable since the OBC cannot uniquely identify detected stars in the presence of such large pointing estimate errors in normal operation. The maximum encountered instantaneous pointing estimate error using EWM was 15.9 arcsec which is well within the limit that can be accommodated by EWM.

The redundant SM gave predicted instantaneous pointing estimate errors outside the limit of SM/OBC EWM, due to the reduced number of processed inclined slit star detections. However, simulations performed using a redundant SM with vertical slit star detection supressed showed a performance comparable with that achieved by the operational SM. Therefore the redundant SM is considered to use only the inclined slits.

4.2.3 Occultation. An occultation is a period during which the RTAD algorithm does not receive any SM information. The specification requires two such periods each lasting 15 minutes, separated by 5 minutes with SM data. The pointing estimate error at the end of the second period with no SM information is to be below 5 arcsec (SM/OBC normal mode limit).

With no SM information available the RTAD drift estimates were extremely poor leading to unacceptably large pointing estimate errors, of the order of 50 arcsec, at the end of occultation. In order to improve the RTAD drift estimates, ground calculated mean and final drift estimates for the two occultation periods were used. The mean drift estimate was calculated by averaging the RTAD drift estimates for the occultation period over several skyslices, assuming telemetered drift estimates available every 10 seconds. The resultant mean drift rates were then corrupted by 0.01 arcsec/sec to account for worst case curve fitting errors. The final drift estimates were similarly corrupted. These pessimistic estimates were then incorporated into the simulation.

Two sets of drift estimates were studied:

(1) Perfect drift estimates calculated from

the actual drift given in the simulation.

(2) Curve fitted drift estimates (to allow for worst case errors in the ground calculated drift estimates), Table 4 details the predicted RMS pointing estimate errors for 3 skyslices asssuming no ground drift estimates, perfect ground drift estimates and curve fitted ground drift estimates.

Skyslice	First Period of Occultation			Second Period of Occultation		
	No OGDE	P OGDE	CF OGDE	No OGDE	P OGDE	CF OGDE
PFOV						
1	29.9	1.0	9.7	9.7	0.8	8.9
2	21.4	1.0	9.7	31.9	2.0	7.7
3	24.4	2.0	10.1	38.9	1.2	7.7
FFOV						
1	25.5	0.6	14.9	46.6	2.4	13.4
2	31.5	1.0	13.6	23.5	2.0	11.9
3	11.3	1.0	13.7	33.0	1.5	12.7

Table 3

OGDE : On-ground drift estimates
P-OGDE : Perfect on-ground drift estimates
CF-OGDE : Curve fitted on-ground drift estimates

The predicted occultation results can be summarised as follows:

If ground drift estimates were not used the pointing estimation errors during occultation reached unacceptably large values, of the order of 50 arcsec. The major source of pointing estimation error was the integral of the drift estimate error over the period of occultation. When perfect ground based drift estimates were used very small pointing estimate errors resulted. However, any ground based drift estimate will not be perfect and so a curve fitted ground estimate was used which resulted in pointing estimate error in the region of 15 arcsec. A pointing estimate error of 15 arcsec is outside the limit of normal SM/OBC operation but well within EWM operation and therefore it was apparent that a switch to EWM was necessary after both periods of occultation. Figure 12 shows a typical pointing estimate plot for occultation using a curve fitted ground drift estimate.

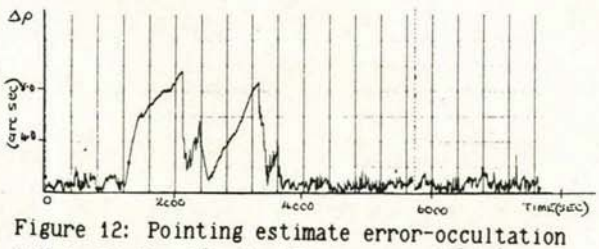

Figure 12: Pointing estimate error-occultation

4.2.4 Station Keeping Manoeuvres. At intervals during the Hipparcos Mission station keeping manoeuvres need to be performed to correct for perturbations in the orbital parameters. This is achieved by continual firing of the ±z thrusters whilst following the NSL. Control action about the z-axis is provided by off-modulation of the ±z-thrusters. Station keeping manoeuvres last up to 1500 seconds during which time no SM updates are available to the RTAD.

The performance measures of interest in this mode are the magnitude of the instantaneous pointing estimate errors at the end of station keeping and the time taken from the end of station keeping to recover nominal RTAD operation again using SM/OBC EWM.

The station keeping manoeuvre was modelled as the maximum duration of 1500 seconds to assess the worst case RTAD performance . For this mode curve fitted on-ground drift estimates, calculated in the manner described in section 4.2.3, were assumed for the station keeping study since the occultation study had shown these were necessary to maintain acceptable pointing estimate errors in the absence of SM updates. The predicted performance assessed over 5 skyslices for the nominal sensor configuration 1240M was as detailed below:

(1) Maximum instantaneous pointing estimate error at the end of the station keeping "burn":-

20.9 arcsec

(2) Averaged pointing estimate recovery time to 5 arcsec:-

450 sec.

The EM study has shown large pointing estimate errors accruing over the period of the station keeping "burn" due predominately to the errors in the curve fitted drift estimates supplied to the RTAD from ground. However, these errors were well within the limit of safe SM/OBC operations and the RTAD performance was shown to recover well in EWM meeting the specification of 600 seconds.

A typical plot showing the PFOV pointing estimate error for one skyslice is given in Figure 13.

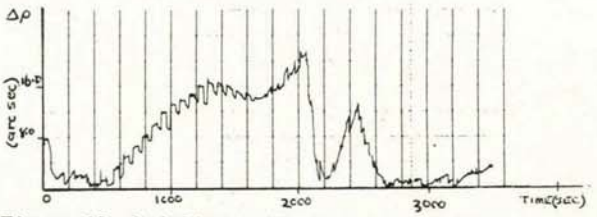

Figure 13: Pointing estimate error-station keeping

4.2.5 Initialisation: Initialisation of the RTAD algorithm is performed in 5 stages:

1) SM and gyro outputs are telemetered to ground from which the spacecraft attitude and gyro drift rates are computed.

2) The ground calculated spacecraft attitude and drift rates are uplinked to initialise the RTAD attitude and drift estimates.

3) The RTAD algorithm operates to determine the spacecraft attitude and drift rates with SM updates being generated on-ground from processed SM telemetry, rather than by the OBC.

4) Once the RTAD performance is compatible with OBC EWM the OBC is activated in EWM to produce the RTAD SM updates, thus replacing the ground action.

5) Once the RTAD performance is compatible with OBC Normal Mode a switch is made to commence normal RTAD operations.

The performance of the RTAD for stages 3 and 4 was determined by computer simulation and is discussed below.

The most significant parameter affecting the RTAD performance during the 3rd stage of initialisation was the 60 second delay between star detection and utilisation of that star information within the RTAD. The large delay time (c.f. 0.5 to 2.0 for normal operation) induced large extrapolation errors into the SM derived update factor used by the RTAD (see Section 3.2.1.2). As a result new fixed gain matrices were calculated specifically for this stage of initialisation. The gains obtained reflected the reduced confidence in the star updates and also showed little difference between category 1 and 2 updates due to the dominance of the extrapolation error on the SM update errors. The predicted RMS pointing estimate errors (assessed over 5 skyslices) for this stage of initialisation are shown in Figure 14. It can be seen that the achieved performance is compatible with safe transition to EWM operation for stage 4 of initialisation.

(ii) The 4th stage of initialisation was assessed using initial pointing estimate errors in excess of those encountered during the first stage of initialisation and worst case drift rate estimate errors. The RTAD algorithm performed well in EWM rapidly reducing the RMS pointing estimate errors to below 5 arcsec (worst case approximately 1000 secs), Figure 15 shows a typical pointing estimation plot for the second stage of initialisation illustrating the reduction in pointing estimate error during this stage.

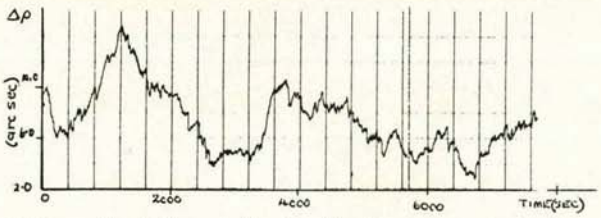

Figure 14: RMS pointing estimate error-stage 3 of initialisation

For safe transition to normal RTAD operations the pointing estimates must be maintained below 5 arcsecs. Figure 15 shows that the RTAD does subsequently maintain the pointing estimate errors below this limit.

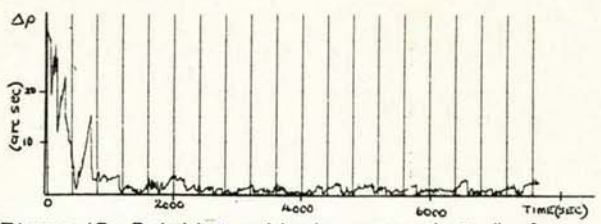

Figure 15: Pointing estimate error-stage 4 of initialisation

4.2.6 Subsystem Test Comparison. The AOCS subsystem performance was assessed by BAe by performing static closed-loop real time tests. The spacecraft dynamics were simulated by the test computer in addition to providing the stimuli to be applied to the sensor electronics. The tests showed the gyro random drift to be outside specification leading to poor drift performance. However, with this taken into account there was good correlation between the test results and the performance predicted by the EM RTAD simulations.

4.3 Protoflight Model (PFM) Performance

At the time of writing the RTAD PFM study is about to commence. A new thermal distortion model has been supplied to BAe, for inclusion in the study, showing largely different thermal distortion data to that used during the EM study. Any possible degradation in normal sunlit performance arising out of the PFM study due to the new thermal distortion model or other PFM data changes is likely to lead to the performance outside the specification. If this were to occur, three possible options could then be investigated to improve the resultant performance:

1) Passive thermal control to improve the thermal distortion profiles (Hardware change).

2) Active thermal control to improve the thermal distortion profiles (Hardware change).

3) Modify the RTAD algorithm to include time varying drift estimates (calibrated on-ground) to reduce the variation between actual drift and RTAD drift estimates (Software change).

5.0 CONCLUSION

The main points of interest arising out of the RTAD EM study are summarised below:

- A two gain sub-optimum Kalman Filter was found to be sufficient to achieve a 1 arcsec RMS telescope pointing performance.

- The performance predicted by the study for normal sunlit operation which covers over 93% of the mission was within the specification.

- For satisfactory eclipse operation EWM was required to accommodate the large pointing estimate errors encountered at eclipse entry and exit. The pointing performance for this mode was predicted to be significantly outside specification. However, eclipse operation represents only about 1.1% of the mission.

- The study showed that for occultation and station keeping it was necessary to use ground calculated drift estimates and switch to EWM at the exit of each mode in order to maintain safe operation. However, it was shown that the recovery of the pointing performance was good in EWM.

- Initialisation was shown, in each stage, to reduce the pointing estimate errors to a level compatible with safe entry to the following stage.

- Finally, good correlation was found between the RTAD predicted results and those shown by the subsystem tests using the EM AOCS units.

ACKNOWLEDGEMENT

This study was conducted by BAe whilst subcontracted to Matra Velizy, who are the Prime AOCS Contractor for HIPPARCOS, an ESA sponsored satellite. Matra Velizy have overall responsibility for the AOCS subsystem .BAe are responsible for the RTAD study, the control law analysis and AOCS subsystem testing.